Proceedings of ASME Turbo Expo 2012
GT2012
June 11-15, 2012, Copenhagen, Denmark

GT2012- 68686

PERFORMANCE OPTIMIZATION OF A 3KW MICROTURBINE FOR CHP APPLICATIONS

W. P. J. Visser
S. Shakariyants
M.T.L. de Later
MTT (Micro Turbine Technology) b.v.
Eindhoven, The Netherlands
wilfried@mtt-eu.nl

A. Haj Ayed
K. Kusterer
B&B-AGEMA GmbH
Aachen, Germany
ayed@bub-agema.de

ABSTRACT

Combined heat and power (CHP) concepts for small scale distributed power generation offer significant potential for saving energy and reducing CO_2 emissions. Microturbines are an interesting candidate for small CHP systems with advantages in terms of performance, size, noise and costs.

MTT has developed a 3kW recuperated microturbine for micro CHP applications, using turbocharger technology for the turbomachinery. In 2010, the development towards a 12.2% efficient demonstrator has been described in [1]. The underlying paper describes the subsequent performance optimization work done to obtain the 18% turbogenerator electric efficiency target.

The work included research focused on improving several components and auxiliary systems resulting in many small loss reduction steps. Combustor performance was improved and emissions reduced. Large steps were made by improving compressor and turbine performance. Compressor efficiency and pressure ratio were optimized to obtain maximum cycle efficiency. Turbine efficiency was improved by a redesign of the turbine scroll.

A detailed CFD study was performed to predict compressor design adaption effects on performance. A 60° sector model was used including inlet duct, impeller (including tip clearance) and diffusor. With prescribed inlet total pressure and total temperature and by varying the outlet static pressure boundary condition, the stationary flow field has been calculated for several operating points. The calculations have been carried out for both the original design and the adapted design.

Results showed that pressure ratio could be increased from 2.9 up to 3.2 using simple adaptations (from the turbocharger original design) while maintaining isentropic efficiency.

Finally, results of the test program and test analysis work are presented.

NOMENCLATURE

η_e	[%]	Electric efficiency (of turbo generator)
η_{enet}	[%]	Net electric efficiency (for turbo generator with auxiliaries)
η_{shaft}	[%]	Shaft thermal efficiency
$\eta_{is,tot}$	[%]	Total-to-total isentropic efficiency
π_{tot}	[-]	Total pressure ratio
ϕ	[-]	Fuel-to-air equivalence ratio
CO		Carbon monoxide
ETA	[%]	Efficiency
D_{tip}	[mm]	Impeller tip diameter
N	[krpm]	Rotor speed
NOx		Nitrogen oxides
PL	[mbar]	Total-to-total pressure loss
PR	[-]	(Compressor) Pressure ratio
PW	[W]	Generator power
Qloss	[W]	Heat loss
q	[mbar]	Dynamic head
Re	[-]	Reynolds number
Tt5	[K]	Recuperator gas-side total inlet temperature
UHC		Unburnt Hydro Carbons
V	[dm3]	Volume

Subscripts

gen	generator
e	electric
ext	external
net	net
is	isentropic
rec_hot	recuperator hot side

ref	reference
tot	total

Abbreviations

CHP	Combined Heat and Power
EGT	Exhaust Gas Temperature
ISA	International Standard Atmosphere
GSP	Gas turbine Simulation Program
RC	Recuperator
PS	Primary (heat-exchange) surface
PZ	Primary zone (combustor)
TIT	Turbine Inlet Temperature

INTRODUCTION

During recent years an increasing number of attempts to design microturbines below 30kW have started for several applications. An increasing number of applications has emerged that could optimally benefit from a microturbine as a prime-mover. These include combined heat and power, electric vehicle range extenders, personal/mobile power units and unmanned aerial vehicles (UAVs) [2]. The latter application could well represent the most significant business driver, although the military variant will be surely classified.

Combined with the availability of off-the-shelf turbocharger technology for the turbomachinery, these applications suggest interesting business cases that may well finally justify the investments required to sufficiently mature microturbine technology for the market.

BACKGROUND

At MTT Micro Turbine Technology, a 3kW recuperated microturbine for micro CHP applications has been developed using turbocharger technology for the turbomachinery. In 2009, 12.2% electric (generator power) efficiency η_e was demonstrated [1] with the test turbine referred to as 'Mk4'. η_e is defined as the ratio of the generator output power and the fuel input heat rate.

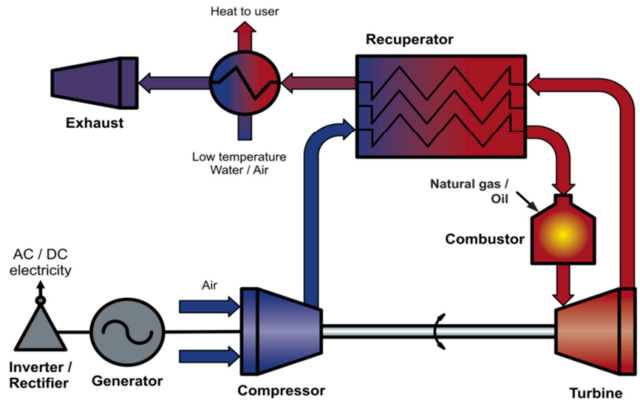

Figure 1: Recuperated microturbine based CHP system.

The next phase included a performance optimization program to increase the net electric efficiency to the design objective of 16.5% net efficiency η_{enet}. This corresponds to about 19.5% η_e or almost 22% shaft thermal efficiency η_{shaft}. Following an assessment of performance improvement potential, separate targets were set for of all components affecting efficiency. A detailed cycle model in the Gas turbine Simulation Program (GSP) [3]-[4] was used to predict effects on cycle efficiency. Parallel projects were launched to work towards the overall objectives.

PERFORMANCE OPTIMIZATION OBJECTIVES

The 12.2% ISA electrical efficiency corresponds to 13.5% shaft (thermal) efficiency when excluding the electrical losses. An improved test turbine has been developed with a different rotor configuration, as shown in Figure 2.

This 'Mk5' test turbine was used for further performance improvement testing and for integration in the micro CHP system prototypes shown in Figure 3. With the Mk5 turbogenerator and CHP system initially comparable performance as with the Mk4 was obtained. When including all CHP sub-system losses (oil, fuel, water pumps, compressors etc.), the net electrical efficiency drops from 12.2% to about 9.5% with a power output of 2000 W. Note that this is due to several non-optimized subsystems consuming excessive power, and that many of these can be relatively easily improved substantially.

Figure 2: Mk5 microturbine.

A Performance Enhancement Program started in November 2010 focused on 3kW at 16.5% net electrical efficiency with separate work packages for the following subsystems and items:

- Bearings
- Recuperator
- Compressor
- Combustor
- Turbine
- Fuel compressor
- Oil pump
- Inlet
- Exhaust
- Ducting
- Heat loss
- Generator
- Inverter

Figure 3: Mk5-based CHP system prototypes in the MTT test cell.

The performance improvement potential of the individual items has been analyzed systematically using available knowledge on technology development from component OEMs, component models and engineering judgement. The GSP cycle model was used to predict the effect on cycle performance. With the efficiencies of the generator and inverter components, the effect on overall efficiency could be determined. Results are shown in Table 1.

Table 1 Performance enhancement objectives and status

Component	Parameter	unit	Initial	Target	$\Delta\eta_{e\,\%}$	Oct. 2011	$\Delta\eta_{e\,\%}$
Recuperator	Δp	%	4.5	4.0	0.22	4.5	0.0
	η	%	85	88	0.8	88	0.8
Bearings	PW_{loss}	W	900	500	1.8	700	0.9
Compressor	PR	-	2.8	3.0	-	3.0	-
	η	%	70	73	1.4	75	2.0
Turbine	η	%	65	67	1.3	70	2.0
Combustor	Δp	%	1.5	1.25	0.1	1.5	
Inlet	Δp	%	1.2	0.75	0.1	1.2	
Exhaust	Δp	%	1	0.75	0.1	1	
Ducting	Δp	%	1	0.75	0.1		
Oil pump	PW_{loss}	W	75	50	0.11	75	
Fuel compr.	PW_{loss}	W	360	300	0.27	300	0.27
Heat loss	Q_{loss}	W	2500	1250			
Generator	PW_{loss}	W	317	215	0.46		
Inverters	PW_{loss}	W	465	328	0.62		
Total					7.38		6.07

When the target improvement would all be realized, a net efficiency increase of 7.35% is predicted. Added to the initial 9.5% net efficiency this would result in 16.85% leaving a 0.35% margin wrt. the design objective. As of October 2011, significant progress was made on the major improvement items as shown in Table 1 resulting in a current net efficiency between 15 and 16%. Electric generator power efficiency η_e, which is directly measured, reached 17.2% ISA. Below follow descriptions of the work done for the individual improvement items.

COMPRESSOR

The compressor has received specific focus for improving performance. Firstly, the pressure ratio at the design speed of 240,000 rpm and about 1300 K TIT had to be increased to the optimal values discussed in the initial development phase: In [1], optimal values of cycle pressure ratio were found to be at least 3 for the optimal cycle efficiency (when assuming also 2+2% recuperator pressure loss). Since with higher pressure ratios, recuperator inlet temperature is reduced and output power increased at the expense of only a slight reduction in efficiency, options to increase compressor pressure ratios up to 3.4 were explored by increasing tip diameter D_{tip}. Next to the reference compressor with diameter D_{tipref} and 2.9 pressure ratio, tip diameters D_{tipref} + 1, D_{tipref} + 2 and D_{tipref} + 3 [mm] were assessed. Prior to testing with these larger diameters, a CFD analysis was performed to assess the effect of increasing D_{tip} by up to 2 mm on performance and to identify design aspects that could be worked on to increase efficiency.

The 240,000 rpm design speed is within the original turbocharger compressor and turbine structural limits and therefore no separate structural analysis was performed at MTT.

COMPRESSOR CFD ANALYSIS

Computational Model

The CFD analysis has been carried out using a commercially available CFD code [16] and has been based on geometric models of the original and the adapted compressor including inlet duct, impeller and diffusor. Both the original and the adapted impeller geometries are shown in Figure 4, where the adaption consisting in extending the impeller blades can be distinguished. Both impeller geometries include the impeller blade tip clearance.

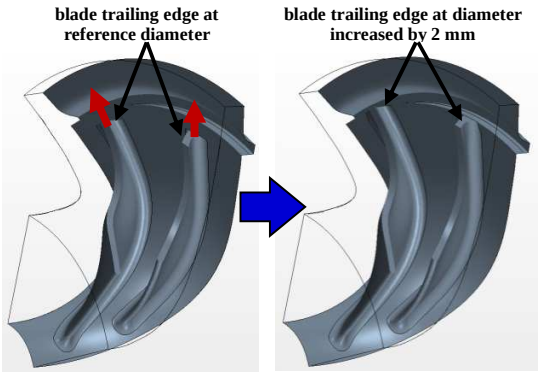

Figure 4: Impeller geometries.

The computation domain has been simplified to a 60° sector making use of the rotational periodicity of the modeled parts. The sector pitch of 60° allows modeling one full blade and one splitter blade within the impeller sector. The non-rotating parts of the model, inlet duct and diffusor, are connected to the rotating impeller part by using mixing plane interfaces. For the CFD calculations a combination of the 3D steady RANS solver and the Spalart Allmaras turbulence model with low y+ wall treatment has been selected. The impeller rotation has been modeled using a rotating reference frame in the impeller part.

The air flow has been treated as ideal gas. The dynamic viscosity has been calculated based on Sutherand's law and the temperature dependence of the specific heat has been considered using a polynomial relation.

The spatial discretization has been performed using a commercially available surface remesher [16] and polyhedral mesher in combination with the prism layer mesher resulting in an unstructured polyhedral mesh featuring layered prismatic cells along the wall boundaries. As a low y+ wall treatment has been selected for turbulence modeling, the thickness of the near wall prism layer has been adjusted, so that y+ values are less than 1 at all near wall cells across the model. The computation grid consists of approx. 370000 polyhedral and prismatic fluid cells in total.

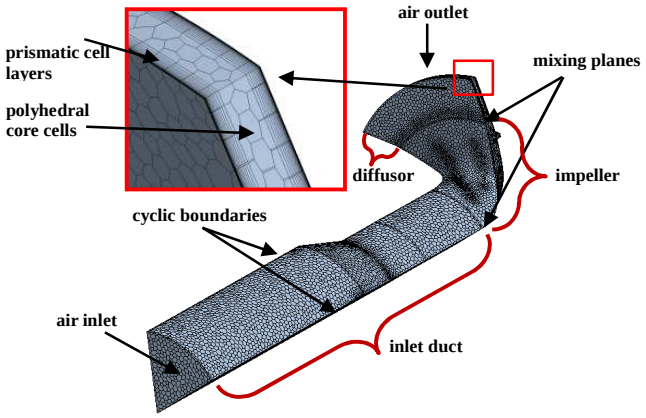

Figure 5: Computational Domain.

Boundary Conditions

The spatial boundaries of the computational domain are shown in Figure 5. Within the present CFD analysis it has been decided to select stagnation inlet and pressure outlet boundaries, where total inlet pressure, total inlet temperature and static outlet pressure are prescribed. Using this combination the inlet pressure level can be kept constant and operating point variation can take place by varying the static outlet pressure. The constant values of total inlet pressure and total inlet temperature are 1.013 bar and 15 °C respectively. The flow direction at inlet has been selected to be normal to the inlet boundary.

The calculations cover four operating points at a rotation speed of 240 krpm and one operating point at a rotation speed of 220 krpm for each compressor configuration.

Results

Figure 6 shows the resulting compressor performance for all calculated operating points. For all calculations satisfactory convergence could be achieved, except for the operating point p2.4 shown in Figure 6, where relatively large fluctuations of mass flow and pressure ratio have been observed during calculation and no sufficient calculation stability could be established. This numerical instability means most probably that the operating point p2.4 is very close to the surge limit of the adapted compressor. The corresponding results of operating point p2.4 given in the figure are average values.

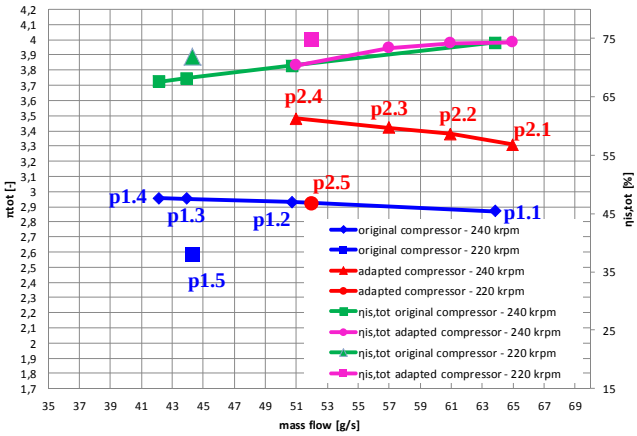

Figure 6: Calculated total pressure ratios and total isentropic efficiencies at Investigated Operating Points.

At a rotation speed of 240 krpm the calculated operating points form corresponding parts of speed lines for each compressor configuration. As expected, the comparison of both speed lines shows a significant increase in total pressure ratio due to the compressor blade extension. For mass flows between 51 g/s and 64 g/s the average increase in total pressure ratio is approx. 17.5%.

The green and the magenta lines show the corresponding total isentropic efficiencies for the original and the adapted compressor, respectively. It can be clearly seen that the efficiencies show similar values for both compressor configurations along the investigated operating range. Also, similar tendency of increased efficiency with increased mass flow can be observed for both configurations.

The speed line of the original compressor (blue line) could be extended to the left by calculating further operating points at lower mass flows. The relatively small slope of the blue line at higher mass flows indicates that the choke limit is clearly higher than 65 g/s. Contrarily, the speed line of the adapted compressor (red line) shows a rather larger steepness at higher mass flows, indicating that choke limit might be at lower mass flows compared to the original compressor. Thus, it can be

expected that the impeller blade extension will lead to a further limitation of the operating range.

A reduction of the rotation speed to 220 krpm shows a decrease in total pressure ratio by approx. 12.5 % to 15.8 % and an increase in total isentropic efficiency by approx. 4.3 % to 5.6 % for the original and the adapted compressor, respectively, at the calculated operating points. Also at this reduced rotation speed the increase in pressure ratio due to the compressor blade extension is not related with a decrease in efficiency. The efficiency seems to be relatively constant for both compressor configurations within the investigated operating range.

An analysis of the flow field inside the compressor shows basically similar flow field characteristics for all investigated operating points. The calculations revealed two loss sources resulting from flow guiding: incidence losses and tip clearance losses in the impeller.

For all operating points a rather positive incidence angle at impeller blade leading edge could be observed, which increases with increasing mass flow.

Figure 7 shows the relative Mach number distribution in a mid-section through the impeller blade leading edge for a mass flow of 63.83 g/s (operating point p1.1). The figure shows that at higher mass flows the stagnation point is shifted from leading edge towards the pressure side resulting in a positive angle of incidence and leading to a strong acceleration on the suction side, where the relative Mach number reaches 1.57 locally and flow separation takes place behind the acceleration zone. As mentioned above, the incidence angle is further increased for higher mass flows consequently resulting in higher incidence losses.

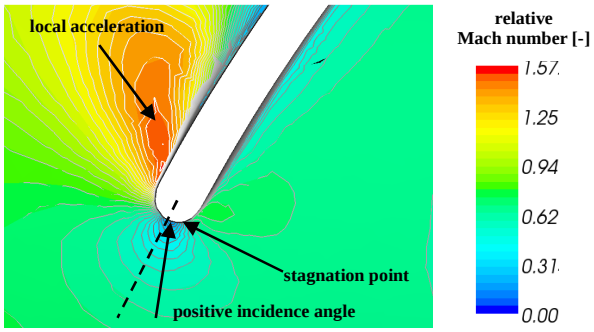

Figure 7: Relative total pressure in a mid-section through impeller blade leading edge (original compressor).

The tip clearance flow has been identified as a major loss source for both compressor configurations. Large vortices inside the impeller passages could be observed, which are mainly caused by the tip clearance flow and which lead to increased blockage and significant pressure loss along the flow passages. The influence of the tip clearance flow is significantly increased with decreased mass flows. The strongest flow passage vortex caused by tip clearance flow has been observed at a mass flow of 42.15 g/s (operating point p1.4) and is shown in Figure 8. The figure shows impeller streamlines in the rotating reference frame from the inlet mixing plane to the diffusor mixing plane. Several streamlines leave the flow passage and flow through the tip clearances of both full blades and splitter blades before forming a large vortex filling a large part of the passage.

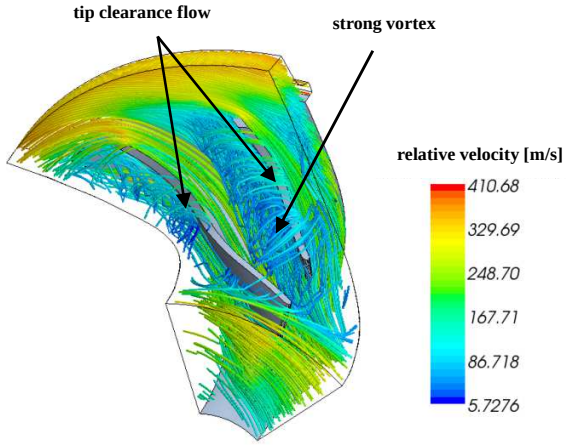

Figure 8: Relative streamlines in the impeller passages.

Altogether, the results of the CFD analysis show that it is possible to increase the total pressure ratio significantly and to maintain efficiency level by extending the impeller blades.

For stationary operation an improvement of the overall compressor performance can be achieved by optimizing the blade leading edge geometry for a given operating point with regards to reduced incidence losses.

Significant improvement can be achieved by reducing the tip clearance height.

TURBINE

The turbine used in the Mk4 test microturbine had only a moderate isentropic (and adiabatic) efficiency of 65%. This was due to both the impeller and scroll design. For the Mk5, a more advanced turbine was available with a maximum reference isentropic efficiency of around 70%. This value is obtained when an optimal scroll design is used, without application design adaptations such as the waste gate or sharp turns in the ducting causing additional pressure losses. Especially for the turbocharger waste gate, aerodynamically smooth turbine exit ducting is often sacrificed. While the Mk4 still had an off-the-shelf automotive application scroll with waste gate, the Mk5 turbine scroll design was optimized and the waste gate omitted. This, combined with the already OEM built in improvements resulted in a 5% increase in isentropic turbine efficiency which was more than anticipated. Since the turbine delivers both the compressor and generator shaft power which is around 13kW, 5% increase means 650W extra power output. However, due to the consequent lower recuperator entry temperature, recuperator heat recovery is reduced somewhat leaving an efficiency increase of around 2%.

COMBUSTOR

Combustor development for a very small recuperated gas turbine is particularly challenged by finding a cost-effective concept for stable and low-emission combustion (NOx vs. CO and UHC). Compared to other applications, the challenges increase due to:

- A range of factors that may promote a flashback and burner overheating:
  - High temperature of the inlet and, consequently, cooling flows in recuperated cycles;
  - Higher surface-to-volume ratios; and
  - Operation without a qualified operator and under a high probability of blunder in the very attractive consumer applications (like domestic CHP);
- Low allowable pressure loss;
- The small scale that limits design choices by the applicability of low-cost (conventional) fabrication methods;
- Low cost requirements for consumer applications; and
- Requirements for a prompt modulation of the operating point.

In the development gas turbines, MTT opted for the "classic" combustor concept with an aerodynamically stabilized diffusion flame. This was justified in order to ensure a durable solution for complete and low pressure loss combustion with wide stability limits to allow testing different designs of other microturbine components (turbomachinery, RC, etc.).

The Mk5 combustor is shown in Figure 9. It was developed by using the common engineering methods [5]-[6]. The predicted performance levels were closely matched experimentally. At the cycle reference point, the operation is characterized by combustion completeness > 0.995, inlet-to-out pressure loss < 1.5 % and PZ intensity ~30 MW/atm-m3. During thermal ramp-up, complete combustion is retained at up 60 MW/atm-m3. Ignition is reliable, including the cold light-off.

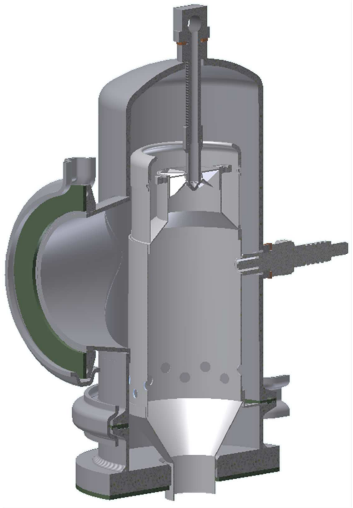

Figure 9: Mk5 combustor.

The Mk5 combustor has a high NOx emission, as shown in Figure 10. It is largely controlled by the inlet temperature, as there is minimal fuel-air premixing. NOx is primarily formed in a nearly stoichiometric vortex breakdown region.

CFD modeling indicated that NOx could be reduced by about 40% by applying dilution holes in the primary zone. The holes were sized and positioned as to avoid quenching of the CO oxidation. The predicted NOx reduction was confirmed with tests, as shown in Figure 10.

Another important factor of NOx formation is the PZ residence time. Figure 10 shows measured NOx reduction in a Mk5 liner with a 20% smaller PZ volume. This limits the thermal power at which complete combustion can be maintained during thermal ramp-up.

For NOx reduction of more than 40-60%, the Mk5 diffusion burner has to be modified by allowing more fuel-air premixing. Various design solutions have been studied. Yet, insufficient flame stability and burner over-heating were observed so far for aerodynamically stabilized flames at inlet temperatures above 920 K (650 °C) – particularly during modulation and transients.

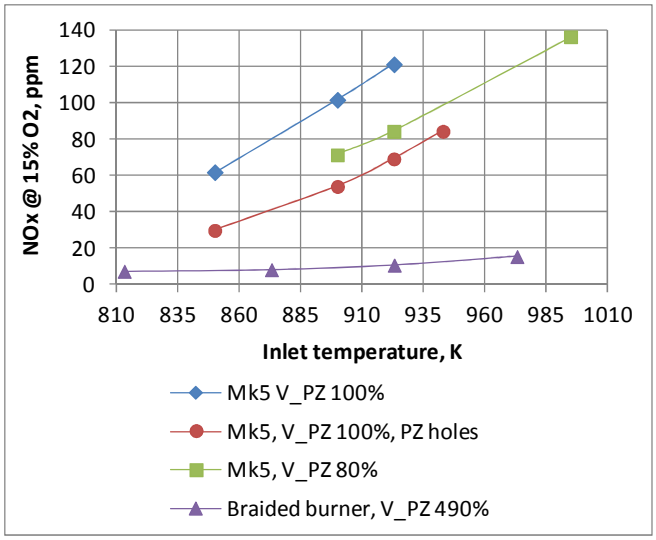

Figure 10: NOx emissions as a function of inlet temperature at ~3 bar and ϕ_PZ 0.5 for the Mk5 combustor and a novel MTT-TU/e braided burner [7].

As an alternative, surface-stabilized flames and ceramic materials have been considered. The new concept of a premix surface burner fabricated by braiding ceramic cords around a ceramic frame was developed, which is presented in [7]. Experimental burners have been extensively tested on a dedicated MTT-TU/e test rig. Low NOx at high inlet temperatures (Figure 10), flame stability within the microturbine operating envelope and structural integrity retention in the short term were demonstrated. R&D on this burner continues, including working towards a complete microturbine combustor demonstrator.

RECUPERATOR

MTT has been working with various OEMs on the development of a high-performance, cost-effective recuperator for the high temperature requirement of the microturbine cycle. Both all-primary surface (PS) and non all-PS types are considered as tradeoffs between the superior effectiveness-specific weight combination of the former [8]-[9] and the structural robustness of the latter.

Various materials are considered along the criteria of life, cost, manufacturability, availability and security of supply. It is widely acknowledged that the common RC steels are not suitable at temperatures above 600-650 °C [10]-[13]. Improved steels, like AL 20-25+Nb, are considered as favorable alternatives that combines good creep strength, oxidation resistance and high formability. Yet, the application upper temperature limit for AL 20-25+Nb is not certain. Ni super alloys, like 625, are very high-performance candidate materials. The Alloy 625 has been extensively tried in microturbine recuperators [8]-[13], yet not up to 800 °C. Ni alloys are, surely, costly and have lower formability compared to stainless steels. Alumina-forming austenitic alloys are emerging as an interesting future material for high-temperatures RCs [14]-[15].

The Mk5 RC is an all-625 cube-shaped plate-pin design, which has replaced a stainless-steel Mk4 all-PS RC [1] on the MTT test turbines. 4 Mk5 recuperator units have been deployed in the development testing at MTT. The longest serving unit has clocked in excess of 100 h at Tt5 800 °C with full retention of structural integrity and performance.

a)

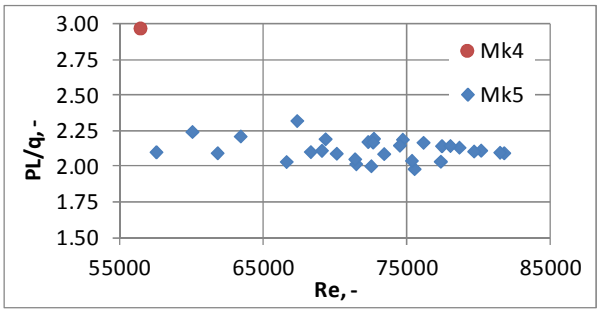

b)

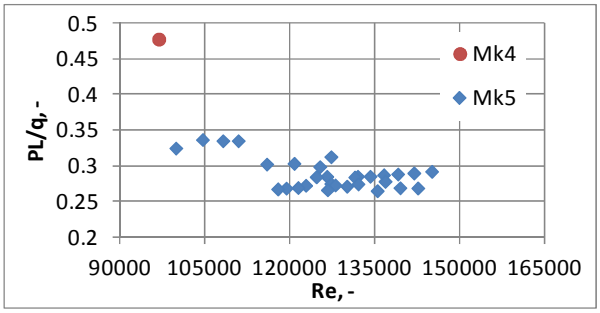

Figure 11: Installed inlet-to-outlet hydraulic resistance (PL/q) of the Mk4 and Mk5 recuperators versus Re: a) air side; b) gas side.

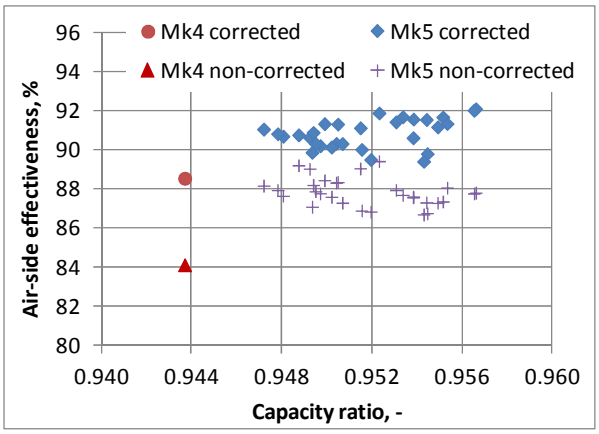

Figure 12: Installed air-side effectiveness of the Mk4 and Mk5 recuperators versus air flow-to-gas flow capacity ratio: with and without correction for heat loss.

Compared to the Mk4 RC, the Mk5 units have a lower installed inlet-to-outlet hydraulic resistance, as shown in Figure 11. The combined relative pressure loss at the cycle reference point is (2.05+2.50) %.

The Mk5 design also has a higher effectiveness, as can been seen in Figure 12: on the order of 88-91 %. In Figure 12, the installed effectiveness is evaluated on the basis of the air-flow enthalpy rise both with and without correction for a heat loss. The correction adds 50% of the heat loss to the air enthalpy rise.

In both Figure 11 and Figure 12, the air and gas properties are evaluated at the mean temperatures, pressures and reference cross sections corresponding to each RC side. The reference flow cross sections the compressor scroll outlet and turbine scroll inlet for the air and gas side respectively.

The recuperator insulation was also improved on the Mk5 microturbine. Porous insulation boards of inorganic silicates with a very low coefficient of thermal conductivity were used. Heat losses were reduced from ~12.7 %/m2 on the Mk4 to 7.0 %/m2 on the Mk5 evaluated as the heat loss relative to the air-flow enthalpy rise divided over the recuperator packaging area.

FUEL COMPRESSOR

The fuel compressor is of the wobble piston type (piston compressor without small-end bearing; the con-rod and the piston are one piece). An off-the-shelf solution was found in an alternative application, that both met the power performance and the low cost requirements. For the efficiency and life requirements a number of relatively simple design adaptations were implemented and tested. This involved modified bearing seals for lower friction and electric motor improvement and resulted in meeting the target power consumption level of 300W and a 0.27% increase in system efficiency $\Delta\eta_e$.

DUCTING

Small pressure loss reductions were projected in the ducting from inlet to exhaust (except for the recuperator for which the pressure loss is addressed separately). These are

implemented in the CHP system demonstrators rather than tested on the experimental rig and only provided small efficiency improvement. Results will be tested on an instrumented prototype later in the development program.

GENERATOR AND POWER ELECTRONICS

Generator and power electronics efficiencies significantly affect net electric performance. Details are considered outside the scope of this paper. In Table 1, power loss values are shown resulting from a separate (generator/electric) optimization study. These values are due to change pending the generator and inverter development program. In general, a 12% total power conversion loss is anticipated from microturbine shaft to power outlet which his equivalent to about 440W. When including auxiliary electric losses over 700W is lost and this means at least 3700W shaft power has to be delivered to the generator.

HEAT LOSS

Heat loss from the hot parts due to conduction, convection and radiation is substantial if insulation measures are not thoroughly implemented. The turbine scroll surface may reach temperatures near or over 1000 °C, turning it into a red hot heat radiator. The combustor is cooler due to the cooler flow around the liner which holds the combustion process. With a recuperated cycle however, this air is preheated (in the MTT cycle up to about 720 °C) thereby increasing potential heat loss. The recuperator is relatively cool on one side and hot at the other, but has a relatively large surface.

Heat loss studies with GSP have shown that with inorganic silicates insulation material cycle performance is significantly improved up to a thickness of 100 mm (Figure 13).

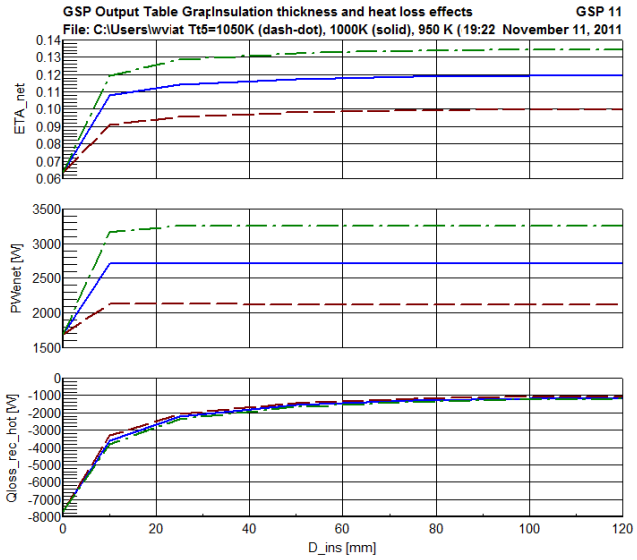

Figure 13: Insulation thickness effect on performance.

From an energy balance calculation, the heat loss from the gas path required to meet the target efficiency is estimated around 1250 W. The latest test heat loss was still 2500 W. It is very difficult to establish an accurate energy balance, particularly around the turbine, so relatively large uncertainty margins have to be accepted. As with the pressure loss, the prototypes will have optimized insulation and are expected to show an efficiency benefit from this in future tests.

While the gas path heat loss is to be minimized, the heat that is still lost should be recovered as much as possible into the CHP system heating circuit. This is done by optimal positioning of the heating water ducting near the heat loss areas. In the heat balance model, heat recovery factors are estimated to determine the overall CHP energy/heating efficiency. This includes heat lost outside the gas path from the oil and generator and bearing cooling circuits, the fuel compressor and power electronics.

An additional requirement to the heat loss is coming from the system heat management perspective. The heat loss will heat up the inside of the CHP system cabinet and to prevent overheating it must be vented to limit temperature. From a cycle calculation it shows that it is more efficient to use a separate fan for this function rather than the compressor inlet air, which, if heated up, would severely penalize microturbine thermal efficiency.

AUXILIARY SYSTEMS

Several auxiliary systems consume electric power thereby reducing net electric efficiency. Outside the ones addressed above (fuel compressor) these include oil pump, cooling/heating circuit water pumps, ventilation fan, control- and user interface electric components. In Table 1, only the oil system is added. The other components only consume very little power and are not yet included in the performance assessment.

TEST RESULTS

Following the analysis work mentioned above, tests have been performed with the improved turbine and different compressor tip diameters. Results are shown in Figure 14 and Figure 15. From the tests, the CFD simulation predictions for compressor pressure ratio and efficiency were confirmed and efficiency was maintained with higher tip diameters. It is clear that with larger tip diameter and the consequent larger pressure ratio, power output increases significantly. Tip diameter D_{tipref} + 1 mm has almost the same cycle efficiency as D_{tipref}. However, beyond tip diameter D_{tipref}+1mm, efficiency drops due to the reduced heat recuperation (see Figure 12 in [1]). From this, it is concluded that at this stage a D_{tipref}+1mm or D_{tipref}+2mm tip diameter must be selected. If during subsequent endurance tests (not covered in this paper), recuperator temperature T5 must be reduced, the (D_{tipref}+3mm) impeller can be used to further reduce Tt5.

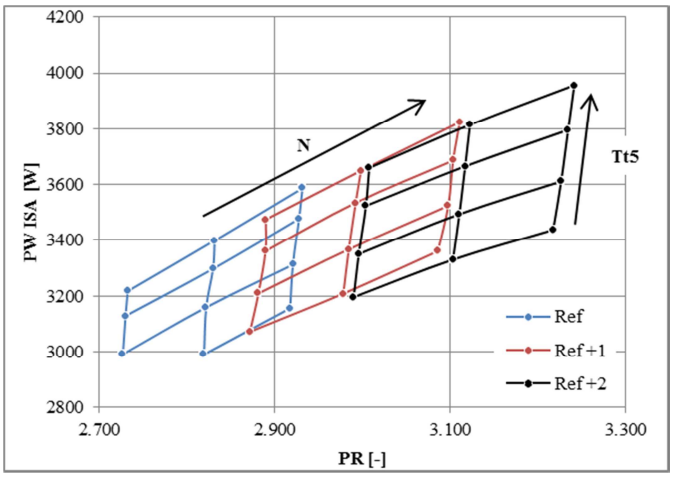

Figure 14: Test results: Generator power (at ISA) versus pressure ratio for different impeller diameters, rotor speed and Tt5.

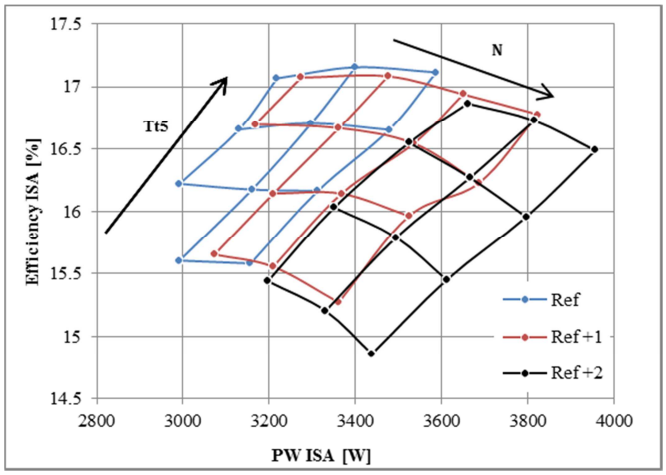

Figure 15: Test results: Electric efficiency vs. generator power (at ISA) for different impeller diameters, rotor speed and Tt5.

NEXT STEPS

Significant progress has been made towards the design objectives and major component improvements have been realized corresponding to the objectives of Table 1. The remaining 1-2% net efficiency improvement required can be covered for a substantial part by working on the smaller items in the table. An effective way towards a larger increase in efficiency is further improving the turbomachinery. The compressor CFD has already hinted at efficiency bottlenecks that offer potential. For the turbine also CFD models will be developed to determine design improvements. These steps will push shaft efficiency beyond 25% and then electric efficiencies of 20% come within reach.

CONCLUSIONS

- The performance enhancement program for the MTT 3kW microturbine has resulted in an increase from 12.2 to 17.2% generator power electric efficiency and 3400W power output.
- Compressor tip diameter increase is an effective means to increase pressure ratio without an isentropic efficiency reduction penalty.
- The compressor CFD analysis has accurately predicted the effect of increasing tip diameter on performance.
- A further 1-2% extra efficiency increase has to be realized to meet the 16.5% net electric efficiency target.
- This objective will be pursued via a turbine efficiency improvement program using CFD modeling similar to the compressor CFD work.
- In addition, small improvement will be made by improving auxiliary component efficiencies and reduce losses.
- This, combined with future developments of turbocharger technology, will provide opportunity to focus on higher efficiencies beyond 20%.

REFERENCES

[1] Visser W.P.J., Shakariyants S.A., Oostveen M., 'Development of a 3kw Micro Turbine for CHP Applications', ASME GT2010-22007.

[2] RTO Educational Notes, 2004, 'Micro Gas Turbines', RTO-EN-AVT-131

[3] Visser, W.P.J. and Broomhead M.J., 2000, 'GSP, A Generic Object Oriented Gas Turbine Simulation Environment', ASME-2000-GT-0002.

[4] GSP website: www.gspteam.com (11-11-2011)

[5] Lefebvre A. H., 1999, *Gas Turbine Combustion.* Taylor&Francis.

[6] Mellor A. M., editor, 1990, Design of Modern Turbine Combustors. Academic Press.

[7] Kornilov V., Shakariyants, S., De Goey P., 2011, 'Novel burner concept for premixed surface-stabilized combustion', ASME GT2012-69036.

[8] McDonald C. F., 2000, 'Low-cost compact primary surface recuperator concept for microturbines', 20, App. Th. Eng., 23, pp. 471-497.

[9] McDonald C. F., 2003, 'Recuperator considerations for future higher efficiency microturbines', App. Th. Eng., 23, pp. 1463-1487.

[10] Maziasz P. J., Pint B. A., Shingledecker J. P., et.al., 2007, 'Advanced alloys for compact, high-efficiency, high-temperature heat-exchangers, In. J. of Hydrogen En., 32, pp. 3622-3630.

[11] Matthews W. J., More K. L. and Walker L. R., 2008, 'Long-Term Microturbine Exposure of an Advanced Alloy for Microturbine Primary Surface Recuperators', ASME GT2008-50037.

[12] Rakowski J. M., Stinner C. P., M. Lipschutz, J. P. Montague, 2008, 'Environmental Degradation of Heat-Resistant Alloys During Exposure to Simulated and Actual Gas Turbine Recuperator Environments', ASME GT2008-51336.
[13] Aquaro D., Pieve M., 2007, 'High temperature heat exchangers for power plants: Performance of advanced metallic recuperators', App. Th. Eng., 27, pp. 389-400.
[14] Pint B. A., Shingledecker J. P., Brady M. P., and Maziasz P. J., 2007, 'Alumina-forming austenitic alloys for advanced recuperators', ASME GT2007-27916.
[15] Pint B. A., Brady M. P., Yamamoto Y., Santella M. L., Maziasz P. J., and Matthews W. J., 2011, 'Evaluation of alumina-forming austenitic foil for advanced recuperators', ASME GT2010-23003.
[16] Star-CCM+ V6.06 Manual

